Diversity Deconstrains Component Limitations in Sensorimotor Control

Yorie Nakahira

ynakahir@andrew.cmu.edu Electrical and Computer Engineering, Carnegie Mellon University, Pittsburgh, PA 15213, USA

Quanying Liu

liuqy@sustech.edu.cn Biomedical Engineering, Southern University of Science and Technology, Shenzhen, Guangdong 518055, China

Xiyu Deng

xiyud@andrew.cmu.edu Electrical and Computer Engineering, Carnegie Mellon University, Pittsburgh, PA 15213, USA

Terrence J. Sejnowski

terry@salk.edu

The Salk Institute for Biological Studies, La Jolla, CA 92037, USA; and Department of Neurobiology, University of California San Diego, La Jolla, CA 92037, USA

John C. Doyle

doyle@caltech.edu

Computing and Mathematical Sciences, California Institute of Technology, Pasadena, CA 91125, USA

Human sensorimotor control is remarkably fast and accurate at the system level despite severe speed-accuracy trade-offs at the component level. The discrepancy between the contrasting speed-accuracy trade-offs at these two levels is a paradox. Meanwhile, speed accuracy trade-offs, heterogeneity, and layered architectures are ubiquitous in nerves, skeletons, and muscles, but they have only been studied in isolation using domain-specific models. In this article, we develop a mechanistic model for how component speed-accuracy trade-offs constrain sensorimotor control that is consistent with Fitts' law for reaching. The model suggests that diversity among components deconstrains the limitations of individual

Yorie Nakahira is the corresponding author. Nakahira and Liu contributed equally to this article.

components in sensorimotor control. Such diversity-enabled sweet spots (DESSs) are ubiquitous in nature, explaining why large heterogeneities exist in the components of biological systems and how natural selection routinely evolves systems with fast and accurate responses using imperfect components.

1 Introduction

The disparities between the speeds and accuracies of the components engineers use to design control systems and those found in nature are enormous. Electronic systems use transistors with a nanosecond clock, and nature uses neurons that work on a millisecond timescale. This introduces internal delays in brains a million times slower than digital systems. Another disparity is in the rate at which information can be communicated by slow axons, whose firing rate is limited to less than a kilohertz compared with wires in electronic systems that signal at gigahertz rates. Nonetheless, nature has achieved remarkably adept and adaptive control strategies that are both fast and accurate. The explanation for this paradox has been elusive.

The premise of this study is that nature evolved control systems with architectures that are compatible with the limitations of available components. Previous theories with log and power laws with favorable tradeoffs are common in biological systems, but these are at the behavioral level and do not explain how they are achieved in brains. We focus on a well-established speed-accuracy trade-off for reaching and show how it could be implemented with the known properties of nerves and muscles within a control architecture.

Fitts' law describes a speed-accuracy trade-off for rapidly reaching targets that holds for a wide range of effectors, including the hand, eye gaze, and computer mouse. Because the time required for reaching a target of width W at a distance D empirically scales as $\log_2(2D/W)$ (Fitts, 1954; Fitts & Peterson, 1964; MacKenzie, 2018), faster speed can be achieved with only a small decrease in accuracy. In contrast, the speedaccuracy trade-offs (SATs) of components implementing the control for reaching can be much more severe (Hartline & Colman, 2007; More et al., 2013; More & Donelan, 2018; Sterling & Laughlin, 2015; Perge et al., 2012). Here, SATs refer to the inherent constraint where improving one aspect, such as speed, often comes at the detriment of the other, such as accuracy. In biological systems, SATs at the component level (e.g., neurons, muscles) are typically highly restrictive, limiting the performance of each individual part. Improving both the speed and accuracy of nerve signaling or muscle actuation requires profligate biological resources (see Figure 1); as a consequence, very few nerves or muscles are both fast and accurate (Sterling & Laughlin, 2015).

What are the mechanisms underlying the contrasting SATs at the component and behavioral levels that deconstrain the hard limits of components?

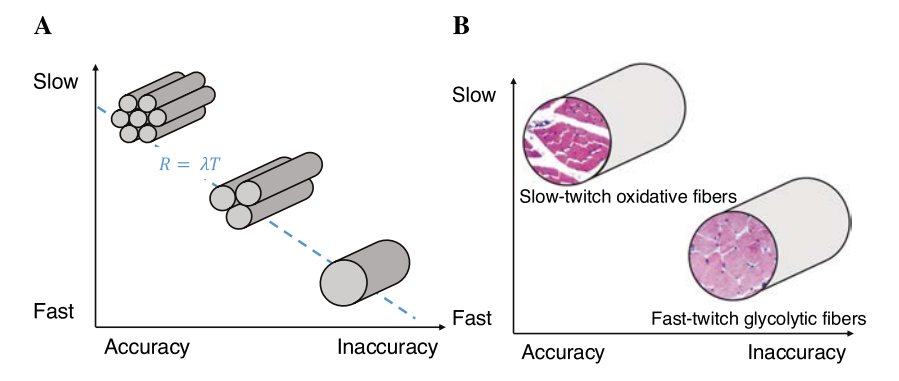


Figure 1: Component speed-accuracy trade-offs (SATs) in nerve signaling and muscle actuation. The horizontal axes show accuracies, and the vertical axes show speed. (A) Axon size-number trade-offs and the resulting SATs. The region above the dashed line represents the achievable speed (delay T) and accuracy (rate R) given a fixed total cross-sectional area to contain all axons, which is proportional to λ . (B) Muscle type/property and the resulting actuation SATs. Muscles with a smaller diameter and darker color (indicating larger amounts of myoglobin, mitochondria, and capillary density) contain oxidative fibers, whereas muscles with a larger diameter and lighter color contain glycolytic fibers. Oxidative fibers are slower but more accurate than glycolytic fibers. Within the class of fast-twitch glycolytic fibers, there are fibers that use oxygen to help convert glycogen to ATP and fibers that use ATP stored in the muscle cell to generate energy.

To answer this question, we studied the impact of component limitations in sensing and actuation on reaching performance to identify key enablers for fast and accurate system responses. The component limitations were (1) Communication latency, (2) rate of sensory nerve signaling, (3), dynamic range of muscle actuation, and (4) precision of the components.

We show that despite the differences in these mechanisms and their limitations, a single principle can explain how they achieve a high level of behavioral performance: diversity in the latencies and accuracies of the components. This diversity principle is quite general and applies to sensors, nerves, skeletons, and muscle locations and their compositions, yielding dramatic performance improvements when coupled with optimal controllers. These optimal controllers are able to dynamically adjust to the diverse capabilities of the system components, maximizing overall efficiency and effectiveness. This interaction creates diversity-enabled sweet spots (DESSs)—regions of optimal system performance that exploit the natural diversity in component properties, such as varying latencies or accuracies. By leveraging this diversity, systems can achieve more robust and efficient control, even when individual components are constrained by severe speed-accuracy trade-offs.

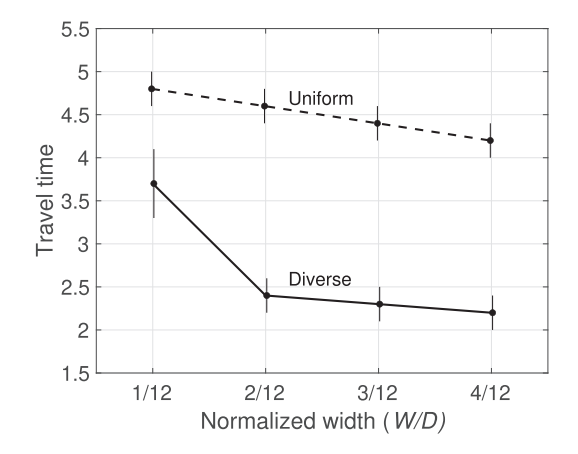


Figure 2: The SATs in uniform versus diverse speed and temporal precision. The predicted reaching times in section 2 are shown for varying normalized width W/D. The predicted reaching time is shown for the uniform cases (equation 2.3) and for the diverse case (equation 2.4). The errors bars indicate the range of possible reaching time due to temporal resolution, and the lines show the predicted values for each condition.

2 Diversity in Speed and Temporal Precision

Our model characterizes the relationships between speed and temporal resolution, the impact of temporal resolution on reaching accuracy, and the impact of speed on reaching time. The model does not include all the complexities in sensorimotor reaching, only the minimum elements necessary to achieve the observed log form of the system SATs. The model we describe generates the reaching SAT in Figure 2. In the model, the diverse case performs much better than the uniform case because the diverse case can use a faster initial speed to move a large portion of the distance as well as a slower final speed to achieve the required accuracy. This speed-accuracy trade-off is qualitatively similar to the ones from Fitts' law, suggesting that speed diversity may underlie the presence of sweet spots in these speed-accuracy trade-offs.

2.1 Reaching Task and Transportation. We consider moving from x = D to a target [-W/2, W/2], which is centered at $x_{\text{target}} = 0$ and has width W, without over- or undershooting. Over- or undershooting is defined as getting into the region $[\infty, -W/2]$ and stopping before arriving (i.e., stopping at $[W/2, \infty]$). Let $\{x(t)\}$ be a reaching trajectory. We are interested in characterizing the travel time, $\min\{T : \dot{x}(t) = 0 \text{ and } |x(t)| \le W/2, \text{ for all } t \ge T\}$, and the settling time, $\min\{T : |x(t)| \le W/2, \text{ for all } t \ge T\}$. We characterize

the speed and accuracy trade-offs when uniform or diverse speeds are allowed for reaching, which also applies to transportation. We limit over- or undershooting in reaching and explicitly model the cost of switching between speeds (which are allowed to take zero or nonzero values), which have qualitative speed and accuracy trade-offs.

2.2 Component Trade-Offs between Speed and Temporal Precision.

Either one or more speeds from $S := \{s_1, s_2, \dots, s_n\}$ can be used to reach a target of width W at a distance D without allowing for over- or undershooting. Without loss of generality, we assume these speeds are indexed in descending order:

$$s_1 > s_2 > \dots > s_n. \tag{2.1}$$

The spatial error e_i , caused by the limited temporal precision in the duration to maintain speed s_i , is defined as the worst-case error in the distance that can be traveled by each speed. Specifically, when x^* is the intended distance to be traveled by speed s_i , the actual distance x can be controlled within the range of $|x - x^*| \le e_i$, where the unit of e_i is the same as the unit used for the distance (or location). We assume that the faster the speeds, the larger the spatial errors: i.e.

$$e_1 \ge e_2 \ge \dots \ge e_n. \tag{2.2}$$

This assumption holds for cases such as Schmidt's law (Schmidt et al., 1979); given a fixed temporal precision, spatial error (the error in location) is proportional to the velocity. We model the switching cost between speeds as a time delay of T_s .

2.3 System Trade-Offs between Time and Precision. From the above definition of spatial error, only speeds whose spatial errors are smaller than $e \leq W/2$ can be used if the final location must be within an interval of width W. Thus, the admissible set of speeds that can reach a target of width W without over- or undershooting is characterized as $S_a(W) := \{s_i \in S : e_i \leq W/2\} \subset S$. Similarly, when one needs to perform multiple reaching tasks whose target width can take any values in a set W, the admissible set of speeds for the target width set W is characterized by $\bigcap_{W \in \mathcal{W}} S_a(W)$.

In the cases of uniform speeds, only one speed is allowed to be used. That speed must be chosen from the admissible set of speeds $\cap_{W \in \mathcal{W}} \mathcal{S}_a(W)$ to avoid over- or undershooting. When the fastest admissible speed, $s_i = \max \cap_{W \in \mathcal{W}} \mathcal{S}_a(W)$ with spatial error e_i is used, one must intend to stop after the state x(t) reaches $W/2 + e_i$ to avoid undershooting. When one intends to stop at $x = W/2 + e_i$, the travel time can range from $(D - W/2)/s_i$ to $(D - W/2 + 2e_i)/s_i$, and the settling time is $(D - W/2)/s_i$. For sufficiently long distance $D \gg W$, both travel time and settling time are dominated by

the term D/s_i and scales with respect to

$$D/\{\cap_{W\in\mathcal{W}}\mathcal{S}_a(W)\} + O(1),\tag{2.3}$$

where O(1) represents the terms that do not scale with D as $D \to \infty$.

In the cases of diverse speeds, multiple speeds can be used. This is particularly beneficial for long distances $(D \gg e_n)$, as one can use the faster speed to travel long distances and slower speed to limit the spatial errors. When a faster speed than the admissible ones $s_k \notin \mathcal{S}_a(W)$ is used, the speed needs to be changed to an admissible one near the target. When one switches to the slow speed (fastest admissible speed) $s_i = \max \mathcal{S}_a(W)$, switching before entering the target at x = W/2 is sufficient for stopping within the target [-W/2, W/2] because the temporal error of the slower speed satisfies $e_i \leq W/2$ by construction. Switching before entering the target at x = W/2 can be ensured by intending to change the faster speed at $x = W/2 - e_k$, given the temporal error of the faster speed e_k . For sufficiently long distance D, when switching is intended at $x = W/2 - e_1$, the travel timescale is with respect to,

$$D/s_1 + O(1)$$
. (2.4)

In equation 2.4, the second term O(1) is determined by the size of W and e and thus does not scale with D as $D \to \infty$. By construction, the distance traveled during the travel time and the settling time differs by at most W, and thus the difference between the travel time and settling time is upperbounded by $\max_{s \in S} W/s$, which does not depend on the distance of the target D. Therefore, the settling time also scales with respect to equation 2.4. Equations 2.3 and 2.4 characterize the scaling of travel times for sufficiently large D for the uniform and diverse cases, respectively. It shall be noted that the diverse case travel time is governed by the fastest speed s_n , whereas that of the uniform case is limited by the admissible speeds.

Next, we consider a special case n=2 and show how the travel times vary with respect to the target width W given D in a way that captures the influence of O(1) term in equations 2.3 and 2.4. In the uniform case, the travel time ranges from $[(D-W/2)/s_i, (D-W/2+2e_i)/s_i]$, where $s_i = \max \cap_{W \in \mathcal{W}} S_a(W)$. In the diverse case, when the faster speed is admissible, that is, $s_n = s_2 \in \mathcal{S}(W)$, the travel time ranges $[(D-W/2)/s_n, (D-W/2+2e_n)/s_n]$. Otherwise, the travel time range is computed as follows. Let d_i and $\hat{d_i}$ be the actual and intended distance traveled by speed s_i , respectively. As stated above, we intend to switch from faster to slower speed at $x = W/2 - e_1$, which in turn gives $\hat{d_1} = D - W/2 - e_1$ and $d_1 \in [D-W/2-2e_1, D-W/2]$. After switching to the slower speed, we intend to stop at $x = W/2 - e_2$ when $D - W/2 > d_1$, or at the earliest possible time otherwise. This gives $\hat{d_2} = \max\{D-W/2+e_2-d_1,e_2\}$ and $d_2 \in [\hat{d_2} - e_2, \hat{d_2} + e_2]$. Thus, the set for $d = (d_1, d_2)$ given the temporal error can be characterized by $\mathcal{D} = \{d: d_1 \in [D-W/2-2e_2, D-W/2], d_2 = (D-W/2-2e_2, D-W/2)$, $d_2 = (D-W/2-2e_2, D-W/2)$, $d_3 = (D-W/2-2e_2, D-W/2)$, $d_4 = (D-W/2-2e_3, D-W/2)$, $d_4 = (D-W/2$

= $[\max\{D - W/2 + e_2 - d_1, e_2\} - e_2, \max\{D - W/2 + e_2 - d_1, e_2\} + e_2]$. Accordingly, the actual travel time is $\{T_d + d_1/s_1 + d_2/s_2 : d \in \mathcal{D}\}$.

2.4 Results. The resulting speed and accuracy of the uniform case and the diverse case are compared in Figure 2. We set D=12, $W=\{1,2,3,4\}$. The pairs of speed and spatial error are set to be $(s_1,e_1)=(2.5,5)$, $(s_2,e_2)=(0.4,0.8)$. For both cases, the error bars show the ranges of travel times and the dots show their centers (midpoints). The above result is reminiscent of how humans can travel with high speed and accuracy using differing means of transportation. The assumptions made in equations 2.1 and 2.2 hold for many means of transportation. For example, flights are fastest but can only land at airports; cars can travel but only stop at the parking lots; and a walker can stop at almost anywhere. The case of traveling by walking, driving, or flying can be modeled by setting the parameters of the above model to be n=3, and s_1, s_2, s_3 being walking driving, and flying speeds, respectively. Comparing equations 2.3 and 2.4 shows that the flexibility to combine walking, driving, and flying enables the traveling time to scale according to s_3 and the resolution to scale according to e_1 .

3 Diversity in Neurons and Muscles

- **3.1 Role of Diversity in Neurons.** SATs for reaching tasks are influenced by the limited communication capacity of the axons in both sensory neurons and motoneurons. Theses axons transmit sensory information through the sensorimotor feedback loop from the periphery to the brain and back to the spinal cord, ultimately activating muscles to execute the task. However, axons within a nerve bundle, as well as across different types of nerves, exhibit a significant degree of heterogeneity, with sizes ranging over two orders of magnitude from tenths to tens of microns (Perge et al., 2012; Stenum, 2018; More & Donelan, 2018). This heterogeneity leads to extreme differences in neural signaling speed and accuracy, as both the speed and rate of information flow in an axon depend on its diameter and degree of myelination (see Figure 1A). In this section, we present a control system model that captures how reaching speed and accuracy is affected by latency and the information capacity of nerve signaling. Our model highlights how diversity in axon composition enhances the speed and precision of reaching movements, a factor not accounted for in traditional Fitts' law models, which typically rely on information theory without considering the tradeoff between information and latency.
- 3.1.1 Reaching Task. We consider the goal of reaching a target as rapidly and accurately as possible. We use $\{x(t)\}_{t=0,1,2,...}$ to denote the trajectory of the cursor, where the coordinate of x(t) is chosen so that the target is located

at the origin. The trajectory is generated by

$$x(t+1) = x(t) + u(t), (3.1)$$

where the change in position over time, x(t+1) - x(t), is determined by the controller and motor actuation u(t). The initial location of the cursor is set to be x(0). We assume that the value of x(0) can only be accessed by the controller after t=0, and its value is smaller than D, that is, $x(0) \in [-D, D]$. The speed of reaching is quantified by the time taken to reach the target T_r , and accuracy is quantified by the normalized width W/D. The target is chosen from a set of disjoint intervals of length W within distance D from the initial location. We define the reaching time as

$$T_r = \{ \tau : |x(t)| \le W/2 \text{ for any } t \ge \tau, |x(0)| \le D \}.$$
 (3.2)

Here, the target is set at the origin of the coordinate of x(t), and the initial location within distance D from the origin (target) lies in [-D, D]. The unit of T_r is the number of sampling intervals, so the actual reaching time is T_r times the sampling interval. The control action is generated using sensing components (e.g., eyes, muscle sensors); communication components (e.g., nerves); computing components (e.g., cortex in the central nervous system); and actuation components (e.g., eye, arm muscles). This model is used to study the performance limitations in two scenarios: when the SATs are bottlenecked by the limitations in nerve signaling (presented in this subsection) and when they are by muscle actuation (see section 3.2). For each scenario, we characterize how the delays and inaccuracies of the neural/motor components affect the performance in reaching.

3.1.2 The SATs in Nerve Signaling. The limitations in nerve signaling are quantified by the signaling delay T_s and rate R in the feedback loop. The delay limits how fast a sensory signal can be reflected on the control action, while the signaling rate limits the amount of information that can be transmitted per unit time. The SATs depend on how the nerves encode information (e.g., spike based, spike rate). Here, we summarize the SATs in spike-based encoding and refer interested readers to Nakahira et al. (2021) for further details and other encoding schemes. In the spike-based encoding scheme, information is encoded in the presence or absence of a spike in specific time intervals, analogous to digital packetswitching networks (Salinas & Sejnowski, 2001; Srivastava et al., 2017). This encoding method requires spikes to be generated with sufficient accuracy in timing, which has been experimentally verified in multiple types of neurons (Mainen & Sejnowski, 1995; Fox et al., 2010). Consider a nerve containing bundles of n axons, each with an average radius ρ . Given fixed resources to build and maintain nerves (axons), there are inherent trade-offs between minimizing signaling delay and maximizing the signaling rate.

Such size versus number trade-offs can be translated into the nerve signaling SATs using the findings from Perge et al. (2009, 2012) and Sterling and Laughlin (2015). When the signaling is precise and noiseless, an axon with an achievable firing rate ϕ can transmit ϕ bits of information per unit time. For sufficiently large myelinated axons, we assume that the propagation speed $1/T_s$ is proportional to the axon radius ρ (Sterling & Laughlin, 2015),

$$T_s = \alpha/\rho, \tag{3.3}$$

for some proportionality constant α . We also model the achievable firing rate ϕ to be proportional to the axon radius ρ ,

$$\phi = \beta \rho, \tag{3.4}$$

for some proportionality constant β . Moreover, the space and metabolic costs of a nerve are proportional to its volume (Sterling & Laughlin, 2015). Given a fixed nerve length, these costs are also proportional to its total cross-sectional area s. Using the above properties, we have

$$R = n\phi = \frac{s}{\pi \rho^2} \beta \rho = \frac{s\beta}{\pi} \frac{1}{\rho} = \frac{s\beta}{\alpha \pi} T_s, \tag{3.5}$$

This leads to

$$R = \lambda T_s, \tag{3.6}$$

where $\lambda = s\beta/\pi\alpha$ is proportional to the spatial and metabolic costs to build and maintain the nerves. This key trade-off between time delay (speed) information rate (accuracy), is illustrated in Figure 1A. Nerve-signaling SATs differ from species to species and in general increase with animal size (More & Donelan, 2018). Bigger animals have more inertia and can tolerate longer delays. They also use more time to compute in part because large animals (e.g., elephants) are more prone to falling.

3.1.3 System SATs in Reaching. The system SATs in reaching, arising from the component SATs, is characterized as follows. The range [-D,D] can hold no fewer than 2D/W disjoint intervals of length W, so the amount of information required to differentiate one interval from other such intervals can be computed as $ID := \log_2(2D/W)$ bits, which equals the Fitts' index of difficulty. This means that after sensing the distance from the target, ID/R time steps are required to deliver ID bits of information from the sensors to the actuators. Then there is a delay of T_s time steps before it is reflected in the actuation. Therefore, the worst-case reaching time cannot be smaller than the sum of the two types of delays, $T_s + ID/R$, yielding

$$\sup_{|x(0)| \in [-D,D]} T_r \ge T_s + \frac{1}{R} \log_2(2D/W) = T_s + \frac{1}{R} ID.$$
(3.7)

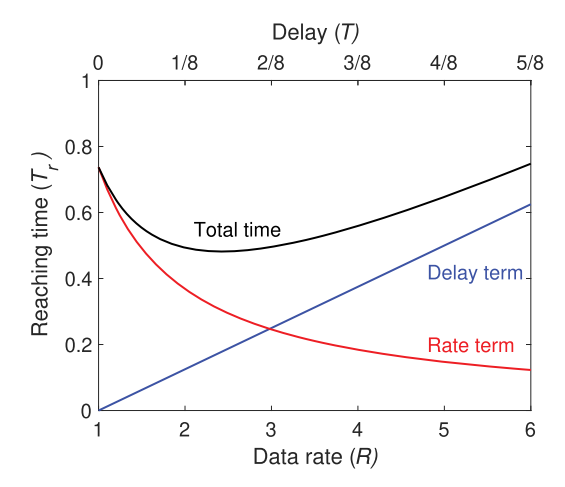


Figure 3: The impact of delay and quantization in reaching time. The lower bound of the reaching time (black) and its composition into the delay term (blue) and rate term (red) from equation 3.12 in section 3.1 are shown for different delays and rates with D=10 and W=3. In the delayed and quantized case, the added delay T and quantization rate R satisfy the SAT T=(R-1)/8.

This provides insights into Fitts' law, $T_r = p + qID$, as follows. The first term, $p = T_s$, is determined by the delay in reacting and transmitting the information on the distance from the target, while q = 1/R is determined from the limited data rate in the feedback loop. Combining equations 3.6 and 3.7 gives a theoretical prediction on how the neurophysiological SATs at the component level affect the reaching SATs (see Figure 3). Specifically, the reaching SAT is given by

$$\sup_{|d| \le D} T_r \ge \frac{1}{\lambda} R + \frac{1}{R} \log_2(2D/W) = \frac{1}{\lambda} R + \frac{1}{R} ID.$$
 (3.8)

Taking the derivative of the right-hand side of equation 3.8 with respect to *R* to zero, we proceed as follows:

$$\frac{d}{dR}\left(\frac{1}{\lambda R} + \frac{ID}{R}\right) = -\frac{1}{\lambda R^2} + \frac{ID}{R^2} = 0. \tag{3.9}$$

$$\therefore R^2 = \lambda ID \tag{3.10}$$

By substituting this into equation 3.6, the minimum reaching time is achieved by

$$R = \sqrt{\lambda ID}, \qquad T_s = \frac{R}{\lambda} = \sqrt{ID/\lambda}.$$
 (3.11)

In the above analysis, we used the component SAT of the form of equation 3.6, but it can be replaced with other formulas for different nerve types or encoding mechanisms.

3.1.4 Fitts' Law. The reaching time under the worst-case target location achievable by the feedback loop with signaling delay T_s and signaling rate *R* is given from equation 3.7 by

$$T_s + \frac{1}{R}\log_2(2D/W) = T_s + \frac{1}{R}ID,$$
 (3.12)

where $ID := \log_2(2D/W)$ is the Fitts' index of difficulty. Equation 3.12 has the form of Fitts' law, and provides a mechanistic interpretation of the individual components of the reaching time. The first term is a function only of delay T_s and is the contribution of delay to the feedback loop (denoted as the delay term). The second term is a function only of the signaling rate R and is the contribution due to limited signaling rate (denoted as the rate term). In equation 3.12, the predicted reaching time depends linearly on the signaling delay T_s and inversely on the signaling rate R (see Figure 3). There also exist component SATs in nerve signaling, and the specific forms depend on various terms such as nerve type, myelination, and resource budget.

Recall that some nerve-signaling SAT can be approximated by $R = \lambda T_s$, where λ is proportional to the spatial and metabolic resources necessary to build and maintain the nerves. The relationship between T_s and R can be used to understand the optimal signaling delay and rate for reaching tasks. Specifically, the minimum reaching time for the combined condition occurs when errors from delays and rate limits are balanced at intermediate speeds and rates, $(T_s = \sqrt{ID/\lambda}, R = \sqrt{\lambda ID})$, rather than at maximum speeds or rates. As the index of difficulty ID increases, the reaching task requires more accuracy, and the relative weight of the rate term to delay term increases. In contrast, minimizing either the delay $(T_s \rightarrow 0)$ or the rate $(R \to \infty)$ alone leads to a large delay term or rate term, and consequently longer reaching times.

Because the optimal T_s and R vary with ID, reaching performance over a broad range of difficulties depends on the diversity in the signaling speed and accuracy of components in the control system. This finding is not contingent on the linearity assumption of the component SATs; other forms of SATs result in different optimal signaling speeds and rates as functions of ID and λ . Nevertheless, diversity remains essential for achieving robust performance over varying difficulties. This requirement may explain the universal presence of heterogeneity in the sizes and number of axons, which mediate a wide range of neural signaling speeds and accuracies (More & Donelan, 2018; Sterling & Laughlin, 2015; Perge et al., 2012).

3.2 Role of Diversity in Motor Units. Another benefit of diversity in the control process occurs in relieving the performance bottleneck due to muscle actuation. Heterogeneity exists in striated muscles, which typically have both larger fast-twitch muscle fibers and smaller slow-twitch muscle fibers (see Figure 1B), and in the wide range of strengths of the motor units (Kernell, 2006; Henneman et al., 1965). Large motor units produce strong forces and shorter rise times, benefiting speed, whereas small motor units are weaker but achieve better accuracy. Motor units are recruited according to Henneman's size principle, recruited from smaller to larger sizes and force for slow movements (Henneman et al., 1965); the recruitment order is more complex and depends on the dynamics of the required muscle strength for fast movements (Marshall et al., 2021). On the other hand, the literature has studied Fitts' laws and reaching behaviors in the context of motor variability (Faisal et al., 2008; Schmidt et al., 1979; Galen & Jong, 1995) and models involving optimizing jerks (Crossman & Goodeve, 1983), smoothness (Crossman & Goodeve, 1983), acceleration (Flash & Hogan, 1985), and kinematics (Plamondon & Alimi, 1997), among others. Although many of these models implicitly capture the component limitations as noise, little study has explored how muscle SATs impose fundamental limits in the speed and accuracy of reaching and how the diversity in motor units affects system behaviors. Here, we characterize how the component SATs in muscle actuation bear on the system SATs in reaching. Specifically, we consider the same setting of the reaching task as in the section 3.1 reaching task. We first model the trade-off between the rise time versus force resolution in muscle actuation. We then translate those into the trade-offs between reaching time versus normalized width. Using this characterization, we investigate the mechanisms behind the use of diversity to deconstrain component limits for obtaining Fitts-like laws.

3.2.1 Component Trade-Offs in Muscle Actuation. A muscle of fixed size has trade-offs in the size and number of motor units in its composition. This number versus size trade-offs give rise to the trade-offs between the speeds and accuracies in motor actuation (see Figures 1B and 4). Specifically, given a fixed space and metabolic resources, the system can build and maintain only many small motor units or a few large motor units. The former achieves better resolution and accuracy (see Figure 4A), while the latter achieves better speed (Figure 4B). We quantify such SAT in actuation using the following model. We consider a muscle with m motor units, indexed by $i \in \mathcal{M} := \{1, 2, \cdots, m\}$. The cross-sectional area of muscle fibers of the motor units affects the biological resources to be used to build and maintain them. We use \bar{F}_i to denote the force that can be produced by the motor unit i and assume without loss of generality $\bar{F}_1 \leq \bar{F}_2 \leq \cdots \leq \bar{F}_m$. Given a fixed fiber length, the maximum force of a muscle ℓ is proportional to its fiber

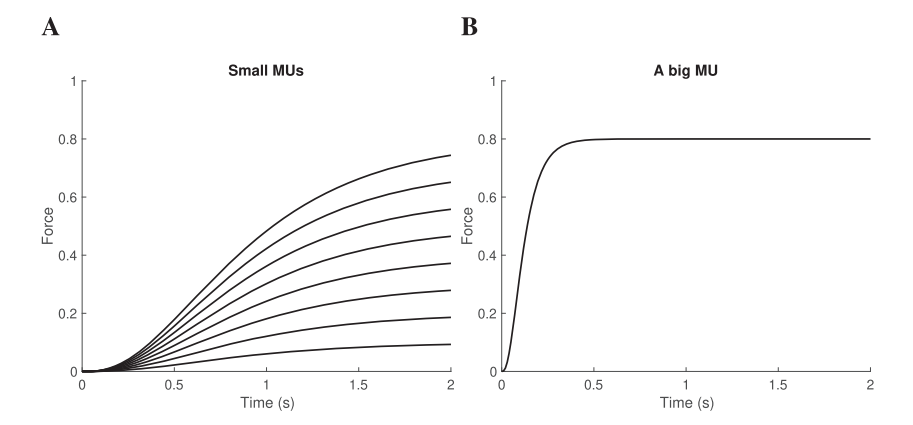


Figure 4: Component-level SATs in muscle actuation. The force rise time uses equation 3.16 from Section 3.2. (A) Force rise time of many small motor units (MUs). The system has eight small motor units of strength level 0.1. The lines show the transient behaviors of the cumulative force levels and their composition. (B) Force rise time of a large motor unit of strength level 0.8. For both cases, the total strength had the same value (0.8) but with different time courses.

cross-sectional area (strictly speaking, myofibril cross-sectional area; Goldspink, 1985; Conwit et al., 1999),

$$\ell = \sum_{i=1}^{m} \bar{F}_i. \tag{3.13}$$

Here we approximate that the maximum force is determined only by the total cross-sectional area of all fibers but not its specific size and number composition. Given a fixed cross-sectional area constraining maximum force, the composition of motor units (and its fiber size and number) determines the speed and accuracy in actuation. The speed of the motor unit *i* can be quantified using the time it takes to rise to its steady-state force F_i after being innervated by its motor neurons. The response dynamics are complex and nonlinear, for which a few models have been proposed (Marieb & Hoehn, 2007; Brezina et al., 2000; Edman & Josephson, 2007; Mendell, 2005). Although the particulars of the models differ by muscle types and neuromuscular parameters, most share three characteristic properties. First, the force response dynamics resembles a sigmoidal function: the contraction begins slowly, becomes faster, and slows down around a steady-state level. Second, motor units with larger fibers and force have greater response speeds. Third, for a fixed total cross-sectional area of motor fibers, composing the motor units with a few larger fibers results in faster response speed than

composing the motor units with many small fibers. Below, we use the model given by Brezina et al. (2000), but we expect our subsequent analysis to produce similar results for other muscle response dynamics with the above three characteristic properties. Brezina et al. characterized the empirical relationship between contraction and firing frequency and conjectured that the relationship between force and firing frequency likely follows a similar form (even though the force of individual motor units cannot be measured).

Based on this relation, the force response dynamics are given by,

$$\dot{a}_i(t) = \alpha f_i^p(t)(1 - a_i(t)) - \beta a_i(t),$$

$$F_i(t) = a_i^q(t),$$
(3.14)

where F(t) is the force, $f_i^p(t)$ is the input (motor neuron firing frequency), $a_i(t)$ is the internal state, and α , β , p, q are fixed constants (Brezina et al., 2000). Note that equation 3.14 satisfies all of the above characteristic properties. In our subsequent analysis, we use the parameter values that Brezina et al. used: $\alpha = 1$, $\beta = 1$, p = 1, q = 3. When motor unit i is recruited at t = 0 for a duration of $\tau_i(\geq 0)$, its force $F_i(t)$ is computed by equation 3.14 with the input

$$f_i(t) = \bar{f}_i \mathbf{1}_{[0,\tau_i]}(t).$$
 (3.15)

Here, $1_I(t) = 1$ if $t \in I$, and $1_I(t) = 0$ otherwise. One can use this relationship to compute how the force level rises after recruitment: setting $\tau_i = \infty$ in equation 3.15 yields

$$F_i(t) = \left\{ \frac{\bar{f}_i}{\bar{f}_i + 1} (-e^{-t(\bar{f}_i + 1)} + 1) \right\}^{1/q} 1(t).$$
 (3.16)

From equation 3.16 the appropriate step input that gives a steady-state force \bar{F}_i is

$$f_i(t) = \bar{f}_i 1_{[0,\infty]}(t),$$
 (3.17)

$$\bar{f}_i = \frac{1}{(1/\bar{F}_i)^{1/q} - 1}. (3.18)$$

To see this, one can notice that a step input, equation 3.17, gives $F_i(t) \to (\bar{f}_i/(\bar{f}_i+1))^{1/q}$ as $t \to \infty$. When we set \bar{f}_i to be equation 3.18, we get the steady-state force $(\bar{f}_i/(\bar{f}_i+1))^{1/q} = \bar{F}_i$.

The speed of muscle actuation is quantified using the time required for the aggregate force generated by all motor units to reach its steady-state values. The steady-state force resolution is quantified using Henneman's size principle (Henneman et al., 1965), which states that motor units in the spinal cord are recruited in ascending order of \bar{F}_i . Thus, a muscle at a non-transient time can only generate m+1 discrete steady-state force levels: 0

and

$$\sum_{i=1}^{n} \bar{F}_i, \quad n \in \mathcal{M}. \tag{3.19}$$

Two example cases for the speed and resolution are illustrated in Figure 4A for the case with many small motor units and in Figure 4B for the case with one big motor unit. The parameters are set to be m=8, $\bar{F}_i=0.1$, and $i\in\mathcal{M}$ for the former, and m=1 and $\bar{F}_1=0.8$ for the latter. In both cases, the total resource use (total cross-sectional area of all motor units) is set to be equivalent, and so is the maximum strength that can be produced by all motor units: $F_{\text{total}}=\sum_{i=1}^m \bar{F}_i=0.8$. The solid lines show $\sum_{i=1}^n F_i(t)$ for $n\in\mathcal{M}$ as a function of time t when all motor units start to be recruited at time t=0. The rising speed of the total force $\sum_{i=1}^m F_i(t)$ is faster when motor units are composed of one big motor unit, whereas the resolution of steady-state force levels $\sum_{i=1}^n F_i(t)$, $n\in\mathcal{M}$ is better with many small motor units.

3.2.2 System SATs in Reaching. The duration of recruitment τ_i in equation 3.15 has a finite temporal resolution. We model the resolution of the recruitment duration τ_i using

$$\tau_i \in \mathcal{T}_s := \{0, t_r, 2t_r, \cdots, \}, \quad i \in \mathcal{M}, \tag{3.20}$$

where t_r can be considered as the temporal resolution. The resolution of recruitment duration in turn limits the resolution in reaching accuracy. This influence can be characterized as below. The dynamics of the reaching distance y(t) can be written as

$$\frac{d^2}{dt^2}y(t) = \sum_{i} (F_i(t) - h(t)),\tag{3.21}$$

given the initial distance y(0) = 0. The function h(t), which captures the friction acting against the motion, takes the form

$$h(t) = \begin{cases} h_s & \text{if } dx(t)/dt = 0\\ h_k & \text{otherwise,} \end{cases}$$
 (3.22)

where h_s can be obtained from the coefficient of static friction and h_k can be obtained from the kinetic friction.

3.2.3 Size Principle in Reaching. Recall that the numbers and sizes of motor units affect force rise time, and resolution in actuation is given in Figures 4A and 4B for systems with many small motor units and one big motor unit, respectively. Here, spatial and metabolic resources to build and maintain them are set to be identical. The force rise time, and resolution can then be translated to reaching SATs as follows. We consider the cases of having two midsized motor units (denoted as the uniform case) or having a large

motor unit and a small one (denoted as the diverse case). While this example uses m = 2, the comparison between uniform versus diverse cases is qualitatively similar for other m. The uniform case has two motor units with the same strength level:

$$(F_1, F_2) = (0.5, 0.5), F_{\text{total}} = F_1 + F_2 = 1.$$
 (3.23)

The diverse case has two motor units with different strength levels:

$$(F_1, F_2) = (0.85, 0.15), F_{\text{total}} = F_1 + F_2 = 1.$$
 (3.24)

For a fair comparison, the sum of steady-state force levels of all motor units $F_{\text{total}} = \sum_{i=1}^{m} \bar{F}_i = 1$ is set to be identical for both cases, so the total resource use (total cross-sectional area of all motor units) is also identical.

The error between the actual recruitment duration τ_i and desired recruitment duration τ^* is given by $\sup_{\tau \in \mathcal{T}_s, \tau^* \geq 0} |\tau - \tau^*| = t_r/2$ from equation 3.20. Let $\mathcal{M}_a(W)$ ($\in \mathcal{M}$) denote the set of the recruitable motor units—motor units that can control the reaching error to be within one-half of the target width. The set $\mathcal{M}_a(W)$ can be evaluated numerically to obtain the achievable forces $\sum_{i \in \mathcal{M}_a(W)} F_i(t)$ and achievable reaching time in Figures 5A and 5B.

Specifically, Figure 5A shows the achievable distance and reaching time given the finite resolution of steady-state force levels in equation 3.19 and that of recruitment durations in equation 3.20. Each dot in Figure 5A shows an achievable distance from equation 3.21 that can be realized by the recruitment dynamics, equation 3.14, with some $\tau_i \in \mathcal{T}_s$, $i \in \mathcal{M}$. The temporal resolution is set to be $t_r = 0.5$. Figure 5B zooms Figure 5A and shows how diversity in motor units benefits reaching. In the case of diverse motor units, large motor units can be used to reach longer distances due to their faster rise time, and small motor units can be used to fine-tune the distance. However, the case of uniform motor units does not have this advantage. Thus, the resolution in achievable distance, given by $\{y(t_f): y(t) = y(t_f), \forall t \geq t_f$, equations 3.14, 3.20, and 3.21} is coarser when the system only has uniform motor units. This is also evidenced by the fact that the dots for the uniform case (black) are sparser than those for the diverse case (red).

Consequently, the reaching SATs are given in Figure 6. In the uniform case, the component trade-offs in muscle actuation directly affect reaching SATs. In contrast, in the diverse case, a sweet spot where faster performance can be achieved with little degradation of accuracy exists. This performance sweet spot is enabled by muscle diversity. Larger motor units can be used to speed to greater distances D, while smaller motor units can be used to accurately control landing on small widths W. Thus, the reaching time decreases sharply as the normalized width (W/D) increases, resulting in an approximately logarithmic SAT curve in reaching. The resulting relation between reaching time and normalized width agrees with the logarithmic trade-offs

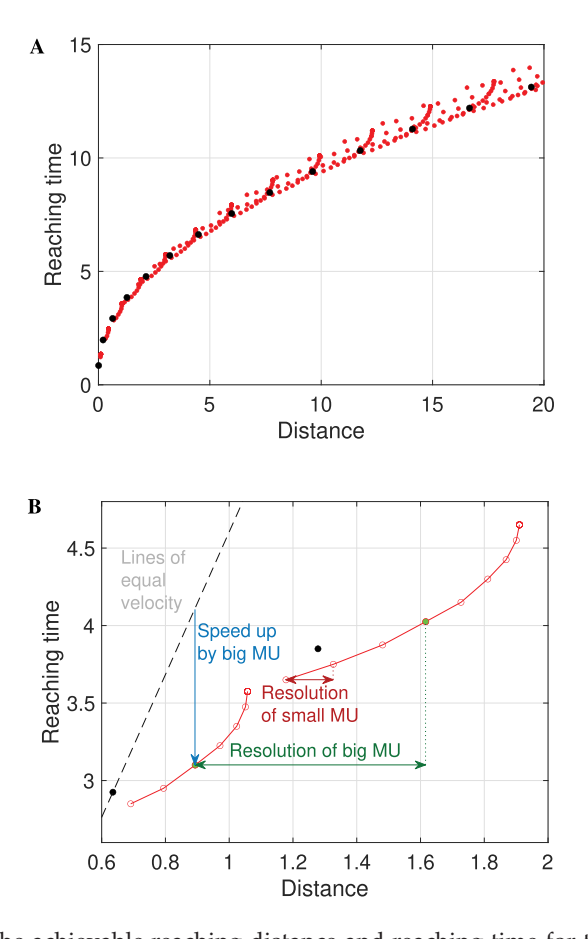


Figure 5: The achievable reaching distance and reaching time for the cases of uniform versus diverse motor units (MU). (A) Plot with all ranges of distance. (B) Zoomed plot on the distance range [0.6, 2]. Each dot represents an achievable pair between the reaching distance and time in uniform case (black) and diverse case (red), based on the model from section 3.2. The pairs with identical contraction duration in both cases are colored in green. The uniform case has two motor units with the same force levels ($F_1 = F_2 = 0.5$), and the diverse case has two motor units with different force levels ($F_1 = 0.85$, $F_2 = 0.15$). The maximum force that can be produced by all motor units is set to be identical in both cases, $F_1 + F_2 = 1$. The muscle contraction duration for each motor unit ranges from 0.75 to 14.75 with a temporal resolution of 0.5. The friction parameters are set to be $h_s = 0.6$ and $h_k = 0.54$. The diverse case has better resolution in distance for the same reaching time because large motor units help reach longer distances due to faster rise time and the small motor units help achieve more precise movements due to their fine-tuning capability.

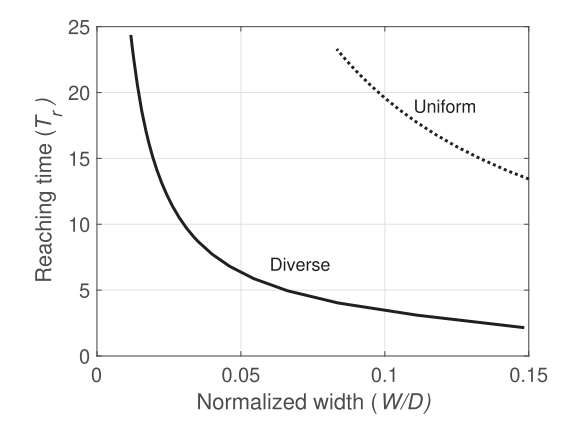


Figure 6: The SATs in reaching arise from uniform vs diverse motor units. The reaching time is obtained by applying the muscle actuation SATs, arising from equation 3.14, in the reaching dynamics in equation 3.21 in section 3.2. The trade-offs between reaching times (speed) and normalized width (accuracy) are shown when muscles are modeled to have uniform motor units (dotted line) or diverse motor units (solid line).

empirically observed in Fitts' law, another result derived from the diversity principle.

4 Discussion

In contrast to the extensive body of research on Fitts' law, which predominantly relies on behavioral-level models, our study focuses on the diversity inherent in sensing and actuation components—a feature ubiquitous in nature—and its impact on sensorimotor performance. We demonstrate that the variation in producible speeds and accuracies of nerve signaling and muscle actuation enhances reaching performance in sensorimotor control. These mechanisms, termed diversity-enabled sweet spots (DeSSs), mitigate physiological constraints to achieve the improved speed-accuracy tradeoffs observed at the behavioral level. Numerous examples of such mechanisms exist in both natural and engineered systems; however, they are often studied in isolation using domain-specific, complex models. The analysis in this article suggests DESSs as a unifying principle for building robust systems with imperfect hardware.

The properties of neurons and muscles have been extensively studied from the perspective of information theory to explain the properties of nerves and muscles that maximize information rates within a fixed energy budget (Hasenstaub et al., 2010; Perge et al., 2012; Hoffmann, 2013; Senn et al., 1997) and minimize the transentropy in sensing (Hatze, 1979).

Information theory has also been used to explain Fitts' law where the movement amplitude is the signal and the target width is the noise (Fitts, 1954; Hoffmann, 2013). These models are macroscopic explanations based on information and communication and are analogous to entropy in thermodynamics. While they can capture important high-level behavioral phenomena, they fall short of explaining how robust control performance emerges from the intricate interactions of diverse physiological components at the microscopic level. Moreover, maximizing neither information nor speed optimizes the control performance of the entire system, which requires balancing the trade-offs between speed and accuracy.

Many control models for reaching have been proposed previously, including two-component, discrete step, step response, iterative-correction, submovement, overlapping impulse, mass-spring, and impulse variability models, some of which involve visual feedback or feedforward motor programs (Hoffmann, 2013; Meyer et al., 2018; Elliott et al., 2017; Crossman & Goodeve, 1983; Takeda et al., 2019; Gawthrop et al., 2008; Schmidt et al., 1979). In these models, logarithmic trade-offs arise from mechanisms (not mutually exclusive) such as corrective submovements (a constant ratio of the remaining distance is traveled with each submovement; Crossman & Goodeve, 1983), force-time curves (Schmidt et al., 1979), signal-dependent noise (Takeda et al., 2019), predictive control (Gawthrop et al., 2008), and proprioceptive or visual feedback (Schmidt et al., 1979). However, all of these explanations are at the macroscopic level, and none take into account the underlying physiological properties of neurons and muscles and their SATs. These behavioral control models are a consequence of the microscopic constraints.

By focusing on the physiological substrates of control, we derived an integrated model where behavior arises from the underlying properties of the components and their constraints, a microscopic model, in the same way that thermodynamics can be derived from statistical mechanics. In our model, macroscopic behavior arises from the detailed architectural features of distributed control theory based on the extreme diversity in the organization of components in nerves and muscles. Both levels of description are useful, just as statistical mechanics and thermodynamics both provide valuable insights into the physics of heat. The statistical mechanics analogy is a familiar example from physics to illustrate the microscopic and macroscopic levels of analysis. However, both thermodynamics and statistical mechanics assume homogeneous microscopic substrates, so the gap between them is much smaller than the gap between the latter in our models, which are diverse in every respect and fragile to random rearrangements at the microscopic substrate level. Specifically, our approach shows how microscopic diversity in neural and muscular components can be exploited to achieve good performance over a broad range of conditions and difficulties. This is a general principle that extends beyond our reaching example. This article only hints at how the architecture of a system can deconstrain

performance from underlying mechanisms (Nakahira et al., 2021; Matni et al., 2024).

This need for diversity may explain why there are orders of magnitude differences in the diameters, numbers, and degrees of myelination of axons within mammalian nerve bundles and between different types of sensory nerves (Stenum, 2018; More et al., 2013; More & Donelan, 2018; Sober et al., 2018; Hodgkin, 1954; Hartline & Colman, 2007). A similar heterogeneity is found in the sizes of the motor units and different types of muscles (Kernell, 2006). Rather than arising from randomness, diversity was meticulously selected by genes interacting with environments for behaviors that favor survival. Nature is more clever than we are at deconstraining the constraints of diverse materials at hand to achieve the desired level of performance.

Other types of diversity relevant to reaching include the extreme size diversity in human skeletons and athletic training. Diversity in skeletons, ranging from fingers to hand to shoulder, allows us to combine arms for large movements with hands and fingers for fine articulation. This diversity is reminiscent of how travel is optimized using diverse means of transportation, allowing travel time to scale according to the fastest form of transportation (flying) and accuracy to scale according to most accurate means (walking). Diverse training in speed, accuracy, endurance, and adaptation is essential to realize DeSS in elite athletic competitions. This regimen derives from sports science on periodization, which uses diverse training schedules (load, sets, and repetitions) to optimize the highly diverse biological mechanisms underlying peak performance and prevent the onset of deleterious side effects from overtraining (Turner, 2011). Even golfers use a variety of clubs to get a small ball into a distant, tiny hole: innacurate drivers for long distances, more accurate irons to reach broad greens, and precision putters to sink the hole. There are many other specialty clubs for problematic lies like sand traps.

There are many other logarithmic laws in nature (and their power law versions) (Olsman & Goentoro, 2016): The Weber-Fechner law for the relation between the physical change in a stimulus and the perceived change in human perception (Fechner, 1966); Ricco's law for visual target detection for unresolved targets (Riccò, 1877); Accot-Zhai's law for steering (a generalization of Fitts' law for 2D environments; Accot & Zhai, 1997); the spacing effect of Ebbinghaus for long-term recall from memory (Ebbinghaus, 1885); and the Hick-Hyman law for the logarithmic increase in decision-time to the number of choices (Hick, 1952; Hyman, 1953). These laws have been extensively studied from the perspective of information constraints. As with Fitts' law, developing microscopic theory and mechanistic models for these laws could reveal underlying relations between the component constraints and provide new perspectives on system behaviors.

Although this article has focused on the diversity of components within a single control layer, it is important to highlight the benefits of diversity across control layers and subsystems. For example, Nakahira et al. (2021) studied the layered control architectures used in mountain biking, including oculomotor control that combines a fast vestibular feedforward system for stabilizing against head motion and a slower cortical feedback loop through the visual cortex for tracking moving objects. More broadly, nature employs diversity both within and between control layers, utilizing diversity-enabled sweet spots to overcome the limitations imposed by severe resource and component constraints in sensorimotor control. This perspective of leveraging diversity both within and across control layers offers valuable insights for designing robust autonomous systems with low-cost hardware and constrained onboard resources. Such designs may allow system trade-offs to be improved fundamentally, while traditional calibrationbased engineering approaches commonly optimize parameters within existing trade-offs. Similarly, some of the brittleness observed in deep learning systems with homogeneous components could be mitigated by incorporating components with diverse time delays, signaling rates, and precision.

Acknowledgments __

This research was supported by the National Science Foundation (NCS-FO 1735004 and 1735003) and the Swartz Foundation. Q.L. was supported by a Boswell fellowship.

Resource Sharing

The data sets and code are available from Yorie Nakahira, the corresponding author, on request.

References

- Accot, J., & Zhai, S. (1997). Beyond Fitts' law: Models for trajectory-based HCI tasks. In Proceedings of the ACM CHI Conference on Human Factors in Computing Systems (pp. 295-302).
- Brezina, V., Orekhova, I. V., & Weiss, K. R. (2000). The neuromuscular transform: The dynamic, nonlinear link between motor neuron firing patterns and muscle contraction in rhythmic behaviors. Journal of Neurophysiology, 83(1), 207–231. 10.1152/jn.2000.83.1.207
- Conwit, R., Stashuk, D., Tracy, B., McHugh, M., Brown, W., & Metter, E. (1999). The relationship of motor unit size, firing rate and force. Clinical Neurophysiology, 110(7), 1270–1275. 10.1016/S1388-2457(99)00054-1
- Crossman, E. R. F., & Goodeve, P. (1983). Feedback control of hand-movement and Fitts' law. Quarterly Journal of Experimental Psychology Section A, 35(2), 251–278. 10.1080/14640748308402133
- Ebbinghaus, H. (1885). Memory: A contribution to experimental psychology. Dover.

Edman, K., & Josephson, R. (2007). Determinants of force rise time during isometric contraction of frog muscle fibres. *Journal of Physiology*, 580(3), 1007–1019. 10.1113/jphysiol.2006.119982

- Elliott, D., Lyons, J., Hayes, S. J., Burkitt, J. J., Roberts, J. W., Grierson, L. E., . . . Bennett, S. J. (2017). The multiple process model of goal-directed reaching revisited. *Neuroscience and Biobehavioral Reviews*, 72, 95–110. 10.1016/j.neubiorev.2016.11.016
- Faisal, A. A., Selen, L. P., & Wolpert, D. M. (2008). Noise in the nervous system. *Nature Reviews Neuroscience*, 9(4), 292. 10.1038/nrn2258
- Fechner, G. T. (1966). Elements of psychophysics. Holt.
- Fitts, P. M. (1954). The information capacity of the human motor system in controlling the amplitude of movement. *Journal of Experimental Psychology*, 47(6), 381–391. 10.1037/h0055392
- Fitts, P. M., & Peterson, J. R. (1964). Information capacity of discrete motor responses. *Journal of Experimental Psychology*, 67(2), 103. 10.1037/h0045689
- Flash, T., & Hogan, N. (1985). The coordination of arm movements: An experimentally confirmed mathematical model. *Journal of Neuroscience*, 5(7), 1688–1703. 10.1523/JNEUROSCI.05-07-01688.1985
- Fox, J. L., Fairhall, A. L., & Daniel, T. L. (2010). Encoding properties of haltere neurons enable motion feature detection in a biological gyroscope. *Proceedings of the National Academy of Sciences*, 107(8), 3840–3845. 10.1073/pnas.0912548107
- Galen, G. P., & Jong, W. P. (1995). Fitts' law as the outcome of a dynamic noise filtering model of motor control. Human Movement Science, 14(4–5), 539–571. 10.1016/0167-9457(95)00027-3
- Gawthrop, P., Lakie, M., & Loram, I. (2008). Predictive feedback control and Fitts' law. *Biological Cybernetics*, 98(3), 229–238. 10.1007/s00422-007-0206-9
- Goldspink, G. (1985). Malleability of the motor system: A comparative approach. *Journal of Experimental Biology*, 115(1), 375–391. 10.1242/jeb.115.1.375
- Hartline, D. K., & Colman, D. R. (2007). Rapid conduction and the evolution of giant axons and myelinated fibers. *Current Biology*, 17(1), R29–R35. 10.1016/ j.cub.2006.11.042
- Hasenstaub, A., Otte, S., Callaway, E., & Sejnowski, T. J. (2010). Metabolic cost as a unifying principle governing neuronal biophysics. *Proceedings of the National Academy of Sciences USA*, 107, 12329–12334. 10.1073/pnas.0914886107
- Hatze, H. (1979). A teleological explanation of Weber's law and the motor unit size law. *Bulletin of Mathematical Biology*, 41(3), 407–425. 10.1007/BF02460820
- Henneman, E., Somjen, G., & Carpenter, D. O. (1965). Functional significance of cell size in spinal motoneurons. *Journal of Neurophysiology*, 28(3), 560–580. 10.1152/jn.1965.28.3.560
- Hick, W. E. (1952). On the rate of gain of information. Quarterly Journal of Experimental Psychology, 4, 11–26. 10.1080/17470215208416600
- Hodgkin, A. (1954). A note on conduction velocity. *Journal of Physiology*, 125(1), 221–224. 10.1113/jphysiol.1954.sp005152
- Hoffmann, E. R. (2013). Which version/variation of Fitts' law? A critique of information-theory models. *Journal of Motor Behavior*, 45(3), 205–215. 10.1080/ 00222895.2013.778815
- Hyman, R. (1953). Stimulus information as a determinant of reaction time. *Journal of Experimental Psychology*, 45, 188–196. 10.1037/h0056940

- Kernell, D. (2006). The motoneurone and its muscle fibres. Oxford University Press.
- MacKenzie, S. I. (2018). Handbook of human-computer interaction. Wiley.
- Mainen, Z. F., & Sejnowski, T. J. (1995). Reliability of spike timing in neocortical neurons. *Science*, 268(5216), 1503–1506. 10.1126/science.7770778
- Marieb, E. N., & Hoehn, K. (2007). Human anatomy and physiology. Pearson.
- Marshall, N. J., Glaser, J. I., Trautmann, E. M., Amematsro, E. A., Perkins, S. M., Shadlen, M. N., . . . Churchland, M. M. (2021). *Flexible neural control of motor units*. bioRxiv:2021.05.05.442653.
- Matni, N., Ames, A. D., & Doyle, J. C. (2024). Towards a theory of control architecture: A quantitative framework for layered multi-rate control. arXiv:2401.15185
- Mendell, L. M. (2005). The size principle: A rule describing the recruitment of motoneurons. *Journal of Neurophysiology*, 93(6), 3024–3026. 10.1152/classicessays.00025.2005
- Meyer, D. E., Smith, J. K., Kornblum, S., Abrams, R. A., & Wright, C. E. (2018). Speed-accuracy tradeoffs in aimed movements: Toward a theory of rapid voluntary action. In M. Jeannerod (Ed.), Attention and performance XIII (pp. 173–226). Erlbaum.
- More, H. L., & Donelan, J. M. (2018). Scaling of sensorimotor delays in terrestrial mammals. *Proceedings of the Royal Society B*, 285(1885).
- More, H. L., O'Connor, S. M., Brøndum, E., Wang, T., Bertelsen, M. F., Grøndahl, C., Donelan, J. M. (2013). Sensorimotor responsiveness and resolution in the giraffe. *Journal of Experimental Biology*, 216(6), 1003–1011. 10.1242/jeb.067231
- Nakahira, Y., Liu, Q., Sejnowski, T. J., & Doyle, J. C. (2021). Diversity-enabled sweet spots in layered architectures and speed-accuracy trade-offs in sensorimotor control. *Proceedings of the National Academy of Sciences*, 118(22), e1916367118. 10.1073/pnas.1916367118
- Olsman, N., & Goentoro, L. (2016). Allosteric proteins as logarithmic sensors. *Proceedings of the National Academy of Sciences*, 113(30), E4423–E4430. 10.1073/pnas.1601791113
- Perge, J. A., Koch, K., Miller, R., Sterling, P., & Balasubramanian, V. (2009). How the optic nerve allocates space, energy capacity, and information. *Journal of Neuroscience*, 29(24), 7917–7928. 10.1523/JNEUROSCI.5200-08.2009
- Perge, J. A., Niven, J. E., Mugnaini, E., Balasubramanian, V., & Sterling, P. (2012). Why do axons differ in caliber? *Journal of Neuroscience*, 32(2), 626–638. 10.1523/JNEUROSCI.4254-11.2012
- Plamondon, R., & Alimi, A. M. (1997). Speed/accuracy trade-offs in target-directed movements. *Behavioral and Brain Sciences*, 20(2), 279–303. 10.1017/S0140525X97001441
- Riccò, A. (1877). Relazione fra il minimo angolo visuale e l'intensita luminosa. *Annali di ottalmologia e clinica oculistica*, 6, 373–479.
- Salinas, E., & Sejnowski, T. J. (2001). Correlated neuronal activity and the flow of neural information. *Nature Reviews Neuroscience*, 2(8), 539. 10.1038/35086012
- Schmidt, R. A., Zelaznik, H., Hawkins, B., Frank, J. S., & Quinn Jr., J. T. (1979). Motoroutput variability: A theory for the accuracy of rapid motor acts. *Psychological Review*, 86(5), 415–451. 10.1037/0033-295X.86.5.415
- Senn, W., Wyler, K., Clamann, H. P., Kleinle, J., Lüscher, H.-R., & Müller, L. (1997). Size principle and information theory. *Biological Cybernetics*, 76(1), 11–22. 10.1007/s004220050317

Sober, S. J., Sponberg, S., Nemenman, I., & Ting, L. H. (2018). Millisecond spike timing codes for motor control. *Trends in Neurosciences*, 41(10), 644–648. 10.1016/ j.tins.2018.08.010

- Srivastava, K. H., Holmes, C. M., Vellema, M., Pack, A. R., Elemans, C. P., Nemenman, I., & Sober, S. J. (2017). Motor control by precisely timed spike patterns. *Proceedings of the National Academy of Sciences*, 114(5), 1171–1176. 10.1073/pnas.1611734114
- Stenum, J. (2018). Size slows animals' response to surprise. *Journal of Experimental Biology*, 221(23).
- Sterling, P., & Laughlin, S. (2015). Principles of neural design. MIT Press.
- Takeda, M., Sato, T., Saito, H., Iwasaki, H., Nambu, I., & Wada, Y. (2019). Explanation of Fitts' law in reaching movement based on human arm dynamics. *Scientific Reports*, 9(1), 1–12. 10.1038/s41598-018-37186-2
- Turner, A. (2011). The science and practice of periodization: A brief review. *Strength and Conditioning Journal*, 33(1), 34–46. 10.1519/SSC.0b013e3182079cdf

Received September 2, 2024; accepted February 9, 2025.